LA-UR -86-843

Los Alamos National Laboratory is operated by the University of California for the United States Department of Energy under contract W-7405-ENG-36.

TITLE: QUANTUM MONTE CARLO AND TRANSFER MATRIX CALCULATIONS FOR 1-D EASY-PLANE FERROMAGNETS

AUTHOR(S): G. M. Wysin
A. R. Bishop

SUBMITTED TO: Physical Review B

Los Alamos National Laboratory
Los Alamos, New Mexico 87545

FORM NO 836 R4
ST NO 2629 5/81

Phys. Rev. B 34, 3377 (1986).

Quantum Monte Carlo and Transfer Matrix Calculations for 1-D Easy-Plane Ferromagnets

G. M. Wysin* and A. R. Bishop
Theoretical Division
Los Alamos National Laboratory
Los Alamos, NM 87545

Abstract

We have applied previously used quantum Monte Carlo (QMC) techniques to obtain numerically the thermodynamics of two well-studied quasi-one-dimensional (1-D) easy-plane ferromagnetic models, in the presence of an applied magnetic field in the easy plane. The checkerboard decomposition form of the Trotter approximation to the partition function has been used. Internal energy, specific heat, magnetization and susceptibility have been obtained for model Hamiltonians believed appropriate for spin $S = \frac{1}{2}$ $(C_6H_{11}NH_3)CuBr_3$ (CHAB) and $S = 1$ $CsNiF_3$, in temperature and field ranges where classical theories have predicted soliton-like kink excitations. The $S = \frac{1}{2}$ QMC calculations are verified and superceded by a numerically exact quantum transfer matrix (QTM) technique.

Results for the temperature dependence of the peak in the specific heat verses field are compared with available experimental results. For the model applicable to CHAB, it is found that there is no value of the easy-plane anisotropy parameter from 4% to 10% for which the QTM calculation can adequately reproduce the experimentally obtained peak height and position. On the other hand, the QMC results for the model assumed for $CsNiF_3$ do roughly reproduce the temperature dependence of the experimental peak positions, but not the peak heights. However, statistical errors present in our QMC data are large, and a better method is still needed for computing the quantum statistical mechanics of $S = 1$ systems.

Introduction

Obtaining a correct theoretical description of the low temperature thermodynamics of the easy-plane spin-1 ferromagnet $CsNiF_3$ has been the subject of a number of investigations in recent years, both theoretical[1-6] and experimental.[7-10] More recently, a similar spin-$\frac{1}{2}$ compound, $(C_6,H_{11}NH_3)CuBr_3$, or "CHAB", has inspired even further interest in easy-plane ferromagnets (EPFs), especially because of the possible existence of (or effective consequences of) classical solitary wave excitations in such a low spin quantum chain.[11] A typical model Hamiltonian for a spin-1 EPF is[1]

$$\hat{H}_{S=1} = \sum_{n=1}^{N} [-J\vec{S}_n\cdot\vec{S}_{n+1} + A(\hat{S}_n^y)^2 - g\mu_B\vec{B}\cdot\vec{S}_n] \quad , \tag{1}$$

where J = 23.6 K, A = 9.0 K and g = 2.4 for $CsNiF_3$.[8] N is the number of spins and μ_B is the Bohr magneton. For a spin-$\frac{1}{2}$ EPF, the easy-plane anisotropy must be in the exchange, then the Hamiltonian is usually taken to be

$$\hat{H}_{S=1/2} = \sum_{n=1}^{N} [(-J_x\hat{S}_n^x\hat{S}_{n+1}^x + J_y\hat{S}_n^y\hat{S}_{n+1}^y + J_z\hat{S}_n^z\hat{S}_{n+1}^z) - g\mu_B\vec{B}\cdot\vec{S}_n] \quad . \tag{2}$$

For CHAB, we take[12] $J_x = J_z = 110$ K, $J_y = 104.5$ K and g = 2.0. In both Hamiltonians, we will find it convenient to choose the xz plane as the easy plane, and to apply the field in the z-direction.

Because of the low spin number, quantum effects might be expected a priori to be strong in both these materials. However, it has been customary to apply classical mechanics as a first approximation. With a field in the easy plane which is small in comparison to the anisotropy ($g\mu_B B \ll 2AS$), and at low temperatures ($T \lesssim J$), the continuum limit classical dynamics is approximately described by the sine-Gordon (sG)

equation.[1] Then the possible excitations include small amplitude spin waves, solitons and breathers. Early neutron scattering experiments on $CsNiF_3$ (Ref. 7,8) and TMMC (a similar antiferromagnet with S = 5/2; Ref. 13) were interpreted in terms of a gas of weakly interacting solitons and spin waves. More recently this interpretation has been challenged and the need to include alternative mechanisms[4-6] has been discussed -- for example, including higher order spin wave processes. Also, the soliton-gas model[14] predicts a peak in the soliton specific heat verses field at fixed temperature, whose position and height are proportional to T^2 and T respectively. The T^2 dependence of the peak position is approximately observed in experiments on CHAB and $CsNiF_3$, but the constants of proportionality are only correct if one assumes an "ad hoc" renormalization of the soliton rest mass. There is no consistent fit for the peak heights in either material.

Furthermore, linear stability analyses[15-16] and numerical simulations of the full classical dynamics[17] (without approximating the equations of motion by the sG equation) have shown that there is an intrinsic instability for the solitons, henceforth referred to as kinks, to deviate strongly from sG-like behavior for applied fields greater than a critical field given by $g\mu_B B_c = 2AS/3$. As the field is increased toward the critical field, the spins show an increasing tendency to tilt out of the easy plane, a motion which is assumed small in the sG approximation. The critical fields are around 18 kG for $CsNiF_3$ and 13 kG for CHAB, somewhat above the ranges where most experiments have been done. This spin tilting increases continuously as the field approaches the critical field, and therefore its effects can generally play a role in the dynamics. For fields greater than the critical

field, the kinks move in a direction opposite to that expected of sG solitons; these have been referred to as "backwards" negative effective mass kinks.[17] It is only in the limit of small field and zero velocity that the out-of-plane tilting vanishes, and then the sG approximation becomes exact. Otherwise, the complete classical dynamics is rather poorly described by the sG equation. This behavior of the kinks also has been obtained by a variational Ansatz calculation.[18]

The classical EPF Hamiltonian has been further shown to be inadequate for explaining experimental data through classical transfer matrix (TM) calculations. In particular, TM calculations[6] of specific heat using the full discrete EPF Hamiltonian give results much higher than experiment[10] for $CsNiF_3$, whereas sG theory (with a renormalized rest mass) fits much closer to experiment. Similar results have been found for easy-plane antiferromagnets[19] comparing experiment with classical Monte Carlo results. It has been suggested that quantum mechanics could effectively restrict spins to the easy plane (tilted by zero-point fluctuations), thereby making sG theory more appropriate than the full classical Hamiltonian, even for S = 1/2 CHAB.[20].

There could be several corrections necessary to the classical model, including effects of next-nearest neighbor interactions, impurities or discreteness. Perhaps even a quite different Hamiltonian is necessary, especially since parameters are usually determined from fits to linear properties, whereas soliton bearing systems exhibit intrinsically nonlinear phenomena. Certainly the most obvious question to consider, however, is how to include quantum mechanics in the model. One approach has been to re-insert the quantum mechanics by simply replacing the classical sG equation with its quantized version, then the

leading correction to the classical theory is a reduction of the sG soliton rest mass.[21] More recently, Johnson and Wright[22] reported on the Bethe Ansatz method[23] applied to solving the quantized sG equation relevant to easy-plane ferro- and antiferro-magnets -- a similar rest mass reduction is found, but still theory and experiment for CHAB, $CsNiF_3$ and TMMC disagree (for specific heat, and therefore probably for other thermodynamic properties). These authors point out, in particular, that the corrected classical sG theory, including kink-kink interactions,[24] would require a rest mass increase to bring the calculated specific heat into agreement with experiment for CHAB. This approach of quantizing a particular limit of the full classical Hamiltonian (the sG limit) seems questionable. By so doing, the out-of-plane degree of freedom is not treated properly; it is essentially transformed to a linear degree of freedom. In view of continuing controversies over the importance of out-of-plane classical motions[25] verses the quantization of the sG model, it seems necessary to include both out-of-plane and quantum aspects simultaneously.

One way of achieving this is to use the recently developed Trotter-Suzuki transformation, whereby the thermodynamics of the original 1-D quantum system is mapped onto the thermodynamics of a 2-D classical system.[26] Numerical evaluation of the internal energy, specific heat, etc. is carried out by using either Monte Carlo or transfer matrix methods.[27] Although this will give no direct information about the excitations, (e.g., the question of existence of solitons) it can nevertheless give crucial indications of the importance of quantum effects and the validity of the assumed Hamiltonians.

In this paper we begin with a brief review of the Trotter-Suzuki formalism, which converts the trace operation in the partition function

definition into a discrete path integral, thereby adding one dimension. New Monte Carlo spin-1 updating algorithms will be given,[28] these being somewhat different from the previous spin-$\frac{1}{2}$ schemes.[27] Results relevant to the $CsNiF_3$ model will be presented, and compared with experiment and sG theory. Unfortunately, these S = 1 data have rather large statistical errors making quantitative comparisons of limited value. Methods other than the present QMC may prove to be more precise. One possibility is the "numerically exact" QTM method as studied by Betsuyaku,[29] which will be applied here to the spin-$\frac{1}{2}$ CHAB thermodynamics. We use a technique to extrapolate from the finite size lattice to the infinite limit in both directions on the 2-D lattice, thereby making this preferred over the previous S = $\frac{1}{2}$ QMC method.[30] We find that there is no value of exchange anisotropy from 4% to 10% for which the QTM results for specific heat peaks will agree with experiment. We have, however, tested that the QTM calculation gives results consistent with the QMC calculation. Finally, a method for calculating the S = 1 fundamental matrix elements is sketched in the Appendix;[28] these matrix elements determine the effective energy of the 2-D lattice, and therefore control the Monte Carlo updating.

II. Trotter-Suzuki Formalism: Checkerboard Decomposition

The original 1-D quantum thermodyanmics spin problem is mapped onto an approximately equivalent 2-D classical thermodynamics problem via an application of a generalized Trotter formula, as suggested by Suzuki.[26] First, the partition function Z is defined in terms of a trace

$$Z = \mathrm{tr}\{e^{-\beta\hat{H}}\} = \sum_{\sigma} \langle\sigma|e^{-\beta\hat{H}}|\sigma\rangle \quad , \tag{3}$$

where β is the reciprocal of the temperature T (we use Boltzmann's constant $k_B = 1$) and $\sigma = \{S_n, n = 1,2,3...N\}$, where the S_n are eigenvalues of some appropriately chosen operators, usually $\hat{S}^z_n$. It is generally not known how to compute the required matrix elements in eq. (3), so the Trotter formula[31] is used to approximate the operator by one for which the matrix elements are easier. The generalized Trotter formula for the exponential of a sum of k operators is

$$\exp\left(\sum_{i=1}^{k} \hat{\theta}_i\right) = \lim_{m\to\infty} \left[\prod_{i=1}^{k} \exp(\hat{\theta}_i/m)\right]^m \quad . \tag{4}$$

Typically the integer k is N for what has been called[32] the "real space decomposition," and k can be 2 or 4 or even 6 for the "checkerboard decomposition." The integer m is referred to as the "Trotter index," and represents the number of discrete path integral steps.

The Hamiltonian is written as a sum of two-body operators $H_{n,n+1}$, and it is convenient to assume that each of these two-body operators can be written as a sum of two parts

$$\hat{H} = \sum_{n=1}^{N} \hat{H}_{n,n+1} \quad , \tag{5a}$$

$$\hat{H}_{n,n+1} = \hat{H}^o_{n,n+1} + \hat{V}_{n,n+1} \quad . \tag{5b}$$

Furthermore, the odd and even n two-body operators are summed separately to define four parts of $\hat{H}$ (i.e. k = 4);

$$\hat{H}^o_{\substack{odd\\even}} = \sum_{\substack{n=odd\\even}} \hat{H}^o_{n,n+1} \quad , \quad \hat{V}_{\substack{odd\\even}} = \sum_{\substack{n=odd\\even}} \hat{V}_{n,n+1} \quad , \tag{6a}$$

$$\hat{H} = \hat{H}^o_{odd} + \hat{V}_{odd} + \hat{H}^o_{even} + \hat{V}_{even} \quad . \tag{6b}$$

The mth-order Trotter approximation to the partition function, $Z^{(m)}$, is then defined by

$$Z^{(m)} = \mathrm{tr}\{[(e^{-\frac{\beta\hat{H}^{o}_{odd}}{m}} e^{-\frac{\beta\hat{V}_{odd}}{m}})(e^{-\frac{\beta\hat{H}^{o}_{even}}{m}} e^{-\frac{\beta\hat{V}_{even}}{m}})]^{m}\} \quad . \tag{7}$$

All four operators $\hat{H}^{o}_{odd}$, etc., are sums of commuting operators, and so this is rewritten as

$$Z^{(m)} = \mathrm{tr}\{(\hat{L}_{odd}\,\hat{L}_{even})^{m}\} \quad , \tag{8a}$$

where

$$\hat{L}_{\substack{odd\\even}} = \prod_{\substack{n=odd\\even}} (e^{-\frac{\beta\hat{H}^{o}_{n,n+1}}{m}} e^{-\frac{\beta\hat{V}_{n,n+1}}{m}}) \quad . \tag{8b}$$

Now, (2m-1) complete sets of states are introduced (in addition to that of the trace itself) labeled by $\sigma_r = \{S_{n,r};\ n = 1,2,3\ldots N\}$, $r = 1,2,3\ldots 2m$. The eigenvalues now have both a position index n and a state index r. Then

$$Z^{(m)} = \sum_{\sigma_1\sigma_2\cdots\sigma_{2m}} \langle\sigma_1|\hat{L}_{odd}|\sigma_2\rangle\langle\sigma_2|\hat{L}_{even}|\sigma_3\rangle\cdots\langle\sigma_{2m}|\hat{L}_{even}|\sigma_1\rangle \quad . \tag{9}$$

From (9) it is evident that we have an expression for a classical partition function on a 2-d lattice of size $N \times 2m$:

$$Z^{(m)} = \sum_{\sigma_1\sigma_2\cdots\sigma_{2m}} \prod_{\langle n,r\rangle} e^{-\beta E(n,r)} \quad . \tag{10}$$

Here brackets <n,r> indicate a product restricted to terms in which n and r are both odd or both even, and the 2-D energy function E(n,r) for a block of four spins on the lattice is given by the fundamental matrix element

$$e^{-\beta E(n,r)} = \langle S_{n,r}\ S_{n+1,r}| e^{-\frac{\beta \hat{H}^{o}_{n,n+1}}{m}}\ e^{-\frac{\beta \hat{V}_{n,n+1}}{m}} |S_{n,r+1}\ S_{n+1,r+1}\rangle. \quad (11)$$

The r variable is the new added dimension. Since the only terms which contribute to the energy of the 2-D lattice are restricted to n and r both odd or both even, this has been called a checkerboard decomposition. In what follows the $S_{n,r}$ variables will be eigenvalues of $\hat{S}^{z}_{n}$ operators, for the rth set of states. In the spin-$\frac{1}{2}$ problem these can be $\pm\frac{1}{2}$, while for spin-1 the possibilities are ± 1 and 0.

The 2-D lattice consists of $\frac{1}{2}Nm$ blocks of 4 spins, or "vertices". In the limit $m \to \infty$, $Z^{(m)}$ approaches the exact partition function of the original 1-D quantum system. The 2-D lattice has periodic boundary conditions in the r (or Trotter) direction, as a result of the trace operation. For the Monte Carlo calculations, periodic boundary conditions will also be imposed in the spatial direction. For the transfer matrix calculations, however, it is very advantageous to use free end boundary conditions in the spatial direction.

Expression (11) needs to be modified slightly, since the resulting matrix elements will not in general be symmetric with respect to the interchange of r and r + 1 (i.e. the matrix is non-Hermitian). We redefine E(n,r) and restore this symmetry:

$$e^{-\beta H(n,r)} = \langle S_{n,r}\, S_{n+1,r+1} | e^{-\frac{\beta \hat{V}_{n,n+1}}{2m}} e^{-\frac{\beta \hat{H}_{n,n+1}}{m}} e^{-\frac{\beta \hat{V}_{n,n+1}}{2m}} | S_{n,r+1}\, S_{n+1,r+1} \rangle \quad . \tag{12}$$

This is equivalent to using k = 6 in the Trotter formula. These matrix elements (or vertex weights) for the spin-1 model are calculated in the Appendix. Spin-$\frac{1}{2}$ matrix elements have already been given elsewhere.[26-30]

The properties of the spin-$\frac{1}{2}$ matrix elements have also been discussed.[26-30] It is important to note that zero matrix elements correspond to infinite energies and therefore prohibited states of the 4-spin blocks or vertices. For the spin-1 problem, out of the possible $(2S + 1)^4 = 81$ matrix elements, only 19 are nonzero for the isotropic case in the absence of a field ($A = B_z = 0$). If a field is added parallel to the quantization axis, there will still be only 19 allowed vertices. However, if a field is added perpendicular to the quantization axis, this produces an 81 vertex model. By choosing the quantization axis in the easy plane, parallel to the field, one obtains a 41 vertex model, independent of the size of the field. Since we are interested in studying the field dependence of the thermodynamics, it is most convenient to choose this last case, so that the model under consideration always has 41 allowed vertices. In this way, updating acceptance rates will depend only weakly on the field strength for any chosen spin updating algorithm. For this 41 vertex model, the allowed vertices are the ones which contain an even number of zeroes (or ±1's), and this influences the choice of an appropriate Monte Carlo updating algorithm.

The decision whether to attempt the flipped or unflipped move is based on the number of zeroes, N_o, along the path before the move. For a given initial path, there are 2^{N_o} flipped moves possible, and 2^{P-N_o} unflipped ones, for a total of $2^{N_o} + 2^{P-N_o}$ possible output states. Therefore the flipped moves should be attempted with probability $2^{N_o}/(2^{N_o} + 2^{P-N_o})$, and the unflipped moves should be attempted with probability $2^{P-N_o}/(2^{N_o} + 2^{P-N_o})$. In the absence of any interactions (all vertex weights equal), we have tested that this algorithm generates equal numbers of -1's, 0's and +1's in the lattice, using an equal number of row, column and square moves at randomly chosen locations.

IV. Monte Carlo Details

We used an approximately constant value of $mT \simeq 60$ K, in order to make the errors due to the Trotter approximation reasonably independent of temperature. This necessitates a larger lattice in the Trotter direction at lower T. For the $CsNiF_3$ parameters, in the temperature range 5 K < T < 15 K and field range $0 \leq B_z \leq 10$ kG (in the easy plane), acceptance rates for row and column moves are « 1%, while square moves have larger acceptance rates $\simeq$ 10%. Because of the inefficiency of this method compared to spin-$\frac{1}{2}$, we present data here for only 16 spins, using only square moves.

The initial configuration was taken to be the state with all $S_{n,r} = 0$. Vertex weights were found for a temperature 2T, and then the Monte Carlo algorithm was applied for 3000 to 5000 "steps", where a step involved attempting Nm square moves chosen at random positions; this is two sweeps through the lattice of Nm/2 vertices. The temperature was then lowered to T, new vertex weights were calculated, and the Monte Carlo was begun using the final configuration of the stirring or heating

interval as the initial configuration. The first 64,000 steps were discarded for equilibration, and then data for expectation values were saved for 192,000 steps. Expectation values of the internal energy, specific heat, in-plane magnetization and susceptibility were computed in a manner identical to that for the spin-$\frac{1}{2}$ problem, as expectation values of appropriate derivatives of the vertex weights.[27] Six bins of 32,000 steps were used for estimation of errors. Finally, data from five such calculations were averaged to obtain the results presented here.

At zero applied field, it was found to be difficult to obtain zero average magnetization, due to the strong effective ferromagnetic exchange, especially at low T. This strong exchange, which is also seen in spin-$\frac{1}{2}$ QMC, causes an effective freezing of the QMC algorithm. This was somewhat alieviated by adding a global spin move (where all spins of the lattice are reversed in sign) attempted once every step. At zero field this move is always accepted and the average magnetization must come out as zero. At nonzero fields the move is accepted with probability 1 if $\Delta E \leq 0$ and probability $e^{-\beta\Delta E}$ if $\Delta E > 0$, as for any other elementary move.

V. QMC Results for $CsNiF_3$

Calculations using $CsNiF_3$ parameters were made in the temperature range $5K \leq T \leq 15$ K for fields up to 10 kG. The internal energy, specific heat and in-plane magnetization and susceptibility verses T are shown in Fig. 1, for fields 0, 5 kG and 10 kG. In Fig. 2 we present the changes in energy and specific heat, $\Delta U = U(B) - U(0)$ and $\Delta C = C(B) - C(0)$, to isolate contributions present only under application of

the field (including, but not exclusively, "soliton" contributions). These data have vague peaks and the scatter is considerable. In Fig. 3 the specific heat ΔC verses field B is shown, at temperatures 5, 6, 7, 8 and 9K. Classical sine-Gordon soliton theory predicts a peak in ΔC verses B, whose position (at $B = B_{peak}$) and height (ΔC_{max}) are proportional to T^2 and T, respectively. For these results, it is estimated, very roughly, that the peaks are at fields 2, 4, 5, 7 and 10 kG. We plot B_{peak} verses T^2 in Figure 4, and compare with the sG theory prediction[24] and with the linear fit to the Ramirez and Wolf experimental data.[10] Linear fits to the three are

$$\begin{aligned} B_{peak} &\simeq 0.14\ T^2 - 1.4 \quad , \quad \text{QMC data,} \\ B_{peak} &\simeq 0.131\ T^2 \quad , \quad \text{Ramirez and Wolf experiment,} \\ B_{peak} &= 0.114\ T^2 \quad , \quad \text{sG theory,}^{24} \text{ no mass renormalization.} \end{aligned} \tag{13}$$

Generally the lack of agreement between experiment and sG theory has been attributed to a quantum reduction of the rest mass of the solitons. One can also compare the results of a Bethe Ansatz solution of the quantized sG equation in Ref. 22. Surprisingly the slopes of the QMC and experimental data are in good agreement, although this may be coincidental, especially considering the quality of the QMC data. Also, there is considerable scatter in the QMC data for peak heights verses T; we can draw no firm conclusion from those data.

There are several deficiencies of this QMC calculation, the largest of which is its inefficiency. A better algorithm is needed with higher acceptance rates so that the statistical errors are reduced. There is also a strong tendency for the system to "freeze" at low T; possible

solutions to this problem might include some annealing procedure, or perhaps a different decomposition of $\hat{H}_{n,n+1}$ into $\hat{H}^{o}_{n,n+1}$ and $\hat{V}_{n,n+1}$. The other major problem is the finite lattice size, in both the spatial and Trotter directions. This latter problem is difficult to correct without first tending to the inefficiency problem.

Because of these difficulties, we cannot make any strong conclusions, especially concerning the question of a "quantum soliton" interpretation to the experimental data. Furthermore, it is not possible to verify the applicability and parameters of the presently accepted Hamiltonian for $CsNiF_3$ without a more accurate calculation. It is likely that quantum effects are important here, and further study, possibly by other methods, is needed. As a step in this direction, we present next a quantum transfer matrix calculation for the spin-$\frac{1}{2}$ model of CHAB, where the accuracy is much better and does show that there are some difficulties to be cleared up in the understanding of the Hamiltonian currently considered to be appropriate.

VI. Quantum Transfer Matrix Calculation for S = 1/2

The Hamiltonian in eq. (2) is used here. The Trotter formula applies just as for S = 1, but now the matrix elements are the spin-$\frac{1}{2}$ functions given previously.[27-30] The coordinate system is oriented so that it is an 8-vertex model, although this simplification is in no way necessary.

The computing method used was given by Betsuyaku,[29] who adapted that of Morgenstern and Binder[34] as originally applied to spin glass models, by allowing for the four-spin interactions. It is necesary to choose free boundary conditions in the spatial direction, while periodic boundary conditions are imposed in the Trotter direction as a result of the trace.

Initially the 2^{2m} partial partition functions of the first column ($S_{1,r}$, r = 1,2,3...2m) are stored in memory. Now consider adding the spins $S_{2,1}$ and $S_{2,2}$ to the lattice, in each of four possible states. This adds one 4-spin block to the lattice. Since all the interactions involving $S_{1,1}$ and $S_{2,1}$ in the first column have been taken into account, we can perform the trace over them, and save in memory 2^{2m} partial partition functions labeled by the states of $S_{2,1}$, $S_{2,2}$, $S_{1,r}$, $r \geq 3$. Next, new spins are added at sites $S_{2,3}$, $S_{2,4}$, and thus the trace over $S_{1,3}$ and $S_{1,4}$ can be performed, and the states are now labeled by $S_{2,1}$, $S_{2,2}$, $S_{2,3}$, $S_{2,4}$, $S_{1,r}$ $r \geq 5$. This procedure is continued until the whole second column of spins has been added to the lattice, at which point the partial partition functions saved will be labeled by states of the second column, $S_{2,r}$ r = 1...2m. This procedure is repeated, adding the spins of the 3rd column by pairs, and tracing over the spins of the 2nd column pair after pair. Columns are added iteratively, thereby transferring from the n particle system to the n + 1 particle system. The procedure is stopped after adding the Nth column and taking the trace over it, obtaining the total partition function $Z^{(m)}$ for any specified temperature. Internal energy, specific heat, magnetization and susceptibility are then obtained by taking appropriate derivatives numerically.

The method requires storing the 2^{2m} Boltzmann factors -- for this calculation we have used $1 \leq m \leq 9$. Computing time rises exponentially with m and linearly with N. Presently the practical limit is m = 9 for storage as well as CPU time using a CRAY-1 800K word machine, while $N \gtrsim 100$ is no practical problem.

For 1-D magnets, it has been noted that for large N the total internal energy U scales like $U(N)/N = U_\infty + a/N$ (Ref. 35) where U_∞ and a are constants. Similarly, it has been shown that the leading errors in the Trotter approximation should be proportional to $1/m^2$ (Ref. 36), a result which has been demonstrated in the numerical calculations of Betsuyaku. We have made use of these two facts to extrapolate to the infinite N, infinite m limit. First, for a given value of m, data from N = 8,14,20,26 and 32 was extrapolated to obtain the $N \to \infty$, finite m limit. A weighted least squares linear fit was used, where the weights were proportional to N. See Figure 5 for an example. Then these data, for a series of m values satisfying $JS^2/mT < 1$, were used to extrapolate to the $N \to \infty$, $m \to \infty$ limit (also in Figure 5). Here a weighted least squares linear fit was also made, where the weights were 1, 2.5, 2.5^2, ..., as m increases. The restriction $JS^2/mT < 1$ is necessary since the Trotter errors actually scale with the square of this parameter. Curiously this parameter must be much smaller to obtain good results in an XY model than for a Heisenberg model.[27]

VII. QTM Results for CHAB

First the method was tested for m = 8, N = 32, at 5% anisotropy ($J_y/J_x = 0.95$) to compare with previous spin-$\frac{1}{2}$ QMC data.[28,30] Results for internal energy, specific heat, magnetization and susceptibility all agreed to within about 5% over the temperature range 4 K to 20 K. Then we applied this method to model (2) with anisotropy ranging from 4% to 10%, in order to compare with the experimental specific heat data of Kopinga et al.[11] As for $CsNiF_3$, ΔC is plotted verses field for a series of temperatures, and then the peak position and height are determined

and plotted verses T^2 and T respectively. Some representative ΔC verses B curves are shown in Figure 6, for the case of 5% anisotropy. The data lie on smooth curves, making the determination of peak positions and heights possible. Interpolation, using a parabolic fit to the peaks, provided a simple accurate way to determine the heights and positions. In Figure 7 the resulting B_{peak} and ΔC_{max} are shown, for anisotropies 4%, 5%, 6%, 8%, and 10%, and compared with classical sG theory and experiment.

The drawn curves in Fig. 7 are classical sG theory results using a soliton rest mass $E^o_{sG} = 8(JS^3 g\mu_B B_z)^{1/2}$, that is, with no adjusted parameters, as in Ref. 24. The predictions of classical sG theory are independent of the anisotropy. Expressions given by Sasaki and Tsuzuki[24] include contributions from spin waves, solitons, and soliton-soliton interactions. Their calculations predicts that the general result for a sG ferromagnet is

$$B_{peak} = AT^2 \quad , \quad A = (64 t_m^2 g\mu_B JS^3)^{-1} \quad , \tag{14}$$

where $t_m = T/E^o_{sG} = 0.190$ has determined the peak position. The corresponding peak height is found to be given by

$$\Delta C_{max} = A'T \quad , \quad A' = 0.196/JS^2 \quad . \tag{15}$$

We see that agreement between this classical theory and experiment is fair for B_{peak} but not as good for ΔC_{max}. None of the chosen values of anisotropy for the QTM fit well to the experimental CHAB data over this temperature range. If the sG soliton rest mass is ad-hoc renormalized such that the slopes of the sG theory B_{peak} curves agree with the experimental slope, then the implied changes in the sG theory ΔC_{max} are not

adequate to cause them to simultaneously fit the experimental data. It has not been apparent how to resolve this problem with classical sG theory. The QTM data presented here obviously should require no such quantum renormalization, but nevertheless systematically disagree with experiment.

VIII. Discussion of Results

The lack of efficiency and resulting lack of accuracy of the S = 1 QMC algorithm presented here led us to consider other methods of obtaining the low-temperature thermodynamics, the first of which is a quantum transfer matrix method. This transfer matrix method as introduced by Betsuyaku was applied here to the S = 1/2 CHAB thermodynamics, thereby making earlier S = 1/2 QMC data obsolete, due to the much greater precision of the newer method (i.e. no statistical errors). The results obtained for specific heat with an in-plane field are in disagreement with presently available experimental data. Other values of easy-plane anisotropy, from 4% to 10%, different from the accepted value of 5%, produced no good fit to the experimental data. It continues to be somewhat surprising how well the classical sG theory is capable of explaining the CHAB specific heat data. We have shown that the quantized version of the ferromagnet Hamiltonian gives approximately the same low-T thermodynamics as the classical sG Hamiltonian, for the case of S = 1/2 CHAB. This can be compared with the classical transfer matrix calculations[20] for the ferromagnet Hamiltonians, which give <u>much</u> larger low-temperature specific heat peaks. Apparently the quantum mechanics plays a strong role in restricting the spins to the easy plane (perhaps including a zero-point out-of-plane component) thereby making the classical theory more appropriate than might at first be expected.

Unfortunately, this QTM method cannot be applied in its present form to the S = 1 $CsNiF_3$ problem, essentially because of computer memory limitations. Generally one expects that the errors due to a finite value of m in the Trotter approximation should scale with the parameter JS^2/mT. For the m-extrapolation method to work well, at a given temperature one needs data at several values of m satisfying $JS^2/mT \ll 1$. Coincidentally, $JS^2 \simeq 25$ K for $CsNiF_3$ as well as for CHAB, and since the interesting soliton regimes are both near T = 5 K, one necessarily must use several points for which m > 5. For S = 1/2, the computer memory needed is of the order of $2 \cdot 2^{2m}$ words, which is 520,000 words for m = 9. This size was the practical limit (also in terms of cpu time) of available CRAY-1 machines (800 K words) at Los Alamos. For S = 1, the computer memory needed will be of the order of $2 \cdot 3^{2m}$ words, which is about 1 M word for m = 6. This memory requirement is excessive and yet m = 6 is too small for the extrapolation. The present QTM method cannot be used for this S = 1 problem without taking into account the intrinsic symmetry of the Trotter subsystems of the 2-D lattice (the columns, along the Trotter direction). (See Ref. 36, 37.) Including these symmetries, possibly by using coherent spin states as in Ref. 37, will reduce the number of states being stored, thereby easing the computer memory limitation problem.

Acknowledgements

We especially wish to thank Indu Satija for many helpful discussions. GMW acknowledges his appreciation for the hospitality of CNLS and T-11 at Los Alamos National Laboratory, whose guest he has been during a large part of his graduate studies, and who have provided the computing and other facilities for this work. This work was performed under the auspices of the U.S. Department of Energy.

Appendix I. Calculation of Spin-1 Matrix Elements

The two-site Hamiltonian is broken up into $\hat{H}^o_{n,n+1}$ and $\hat{V}_{n,n+1}$ as

$$-\beta\hat{H}^o_{n,n+1}/m = K(x_n x_{n+1} + y_n y_{n+1} + z_n z_{n+1}) \quad , \tag{A-1}$$

$$-\beta\hat{V}_{n,n+1}/m = -\beta\hat{V}_n/m - \beta\hat{V}_{n+1}/m$$

$$= -\alpha(y_n^2 + y_{n+1}^2) + b(z_n + z_{n+1}) \quad , \tag{A-2}$$

where

$$K \equiv \beta J/m \quad , \quad \alpha \equiv \beta A/2m \quad , \quad b = \beta B/2m \quad , \tag{A-3}$$

and x_n, y_n, and z_n represent spin-1 operators $\hat{S}^x_n$, $\hat{S}^y_n$ and $\hat{S}^z_n$. The motivation here is that $\hat{V}_{n,n+1}$ is a moderate perturbation on $\hat{H}^o_{n,n+1}$ ($2A/J \simeq 0.38$ for $CsNiF_3$), with very weak dependence on the field strength. Matrix elements of the two parts will be found separately; we sketch the method for $\hat{H}^o_{n,n+1}$; the same method can be applied even more easily to $\hat{V}_{n,n+1}$.

The exponential of (A-1) is needed, i.e.

$$\hat{M} = \exp \hat{KM} = \sum_{p=0}^{\infty} \frac{1}{p!} K^p \hat{M}^p \quad , \tag{A-4}$$

where

$$\hat{M} = x_n x_{n+1} + y_n y_{n+1} + z_n z_{n+1} \quad . \tag{A-5}$$

A method is given here which produces $\hat{M}^{p+1}$ from $\hat{M}^p$, using the anticommutator for symmetrizing the algebra;

$$\hat{M}^{p+1} = \frac{1}{2}\{\hat{M}, \hat{M}^p\} \quad . \tag{A-6}$$

By iteratively taking higher powers of $\hat{M}$, it is found that $\hat{M}^p$ will generally involve 8 different simple spin-1 operators, with coefficients of these operators depending on p, so we can write

$$\hat{M}^p = \sum_{k=1}^{8} C_k(p)\, \hat{O}_k \quad . \tag{A-7}$$

The sum is over the 8 operators $\hat{O}_k$. One can use the fundamental commutator

$$z_n = i[x_n, y_n] \tag{A-8}$$

to write all operators in terms of x and y operators. Then the symmetry of $\hat{M}$ with respect to interchange of x and y operators simplifies the calculation. The 8 operators are:

$$\hat{O}_1 = x_n x_{n+1} + \{x \leftrightarrow y\} \quad ; \quad \hat{O}_5 = (xxyy)_n (xxyy)_{n+1} + \{x \leftrightarrow y\} \quad ;$$

$$\hat{O}_2 = x_n^2 x_{n+1}^2 + \{x \leftrightarrow y\} \quad ; \quad \hat{O}_6 = (xyyx)_n (xyyx)_{n+1} + \{x \leftrightarrow y\} \quad ;$$

$$\hat{O}_3 = (xy)_n (xy)_{n+1} + \{x \leftrightarrow y\} \quad ; \quad \hat{O}_7 = (xy)_n (yx)_{n+1} + \{x \leftrightarrow y\} \quad ;$$

$$\hat{O}_4 = (xxy)_n (xxy)_{n+1} + \{x \leftrightarrow y\} \quad ; \quad \hat{O}_8 = (xyyx)_n (yxxy)_{n+1} + \{x \leftrightarrow y\} \quad ,$$

where $\{x \leftrightarrow y\}$ indicates another term with the x and y operators interchanged. The anticommutators of these, divided by two as in (A-6), are

$$\tfrac{1}{2}\{\hat{O}_1, \hat{M}\} = \hat{O}_2 + \hat{O}_3 - \tfrac{1}{2}\hat{O}_4$$

$$\tfrac{1}{2}\{\hat{O}_2, \hat{M}\} = \hat{O}_1 - \hat{O}_3 + \tfrac{1}{2}\hat{O}_4$$

$$\tfrac{1}{2}\{\hat{O}_3, \hat{M}\} = \tfrac{1}{2}\hat{O}_4 - \hat{O}_6$$

$$\tfrac{1}{2}\{\hat{O}_4, \hat{M}\} = \hat{O}_3 - \tfrac{1}{2}\hat{O}_4 + \hat{O}_5 + \hat{O}_6 \tag{A-10}$$

$$\frac{1}{2}\{\hat{O}_5, \hat{M}\} = \hat{O}_4$$

$$\frac{1}{2}\{\hat{O}_6, \hat{M}\} = -\hat{O}_3 + \frac{1}{2}\hat{O}_4$$

$$\frac{1}{2}\{\hat{O}_7, \hat{M}\} = \hat{O}_8$$

$$\frac{1}{2}\{\hat{O}_8, \hat{M}\} = \hat{O}_7 \quad .$$

Inserting (A-7) into (A-6), we see that the $C_k(p+1)$ coefficients are found from the $C_k(p)$ coefficients by two matrix relationships:

$$\begin{bmatrix} C_1 \\ C_2 \\ C_3 \\ C_4 \\ C_5 \\ C_6 \end{bmatrix}_{p+1} = \begin{bmatrix} 0 & 1 & 0 & 0 & 0 & 0 \\ 1 & 0 & 0 & 0 & 0 & 0 \\ 1 & -1 & 0 & 1 & 0 & -1 \\ -\frac{1}{2} & \frac{1}{2} & \frac{1}{2} & -\frac{1}{2} & 1 & \frac{1}{2} \\ 0 & 0 & 0 & 1 & 0 & 0 \\ 0 & 0 & -1 & 1 & 0 & 0 \end{bmatrix} \begin{bmatrix} C_1 \\ C_2 \\ C_3 \\ C_4 \\ C_5 \\ C_6 \end{bmatrix}_p \quad , \tag{A-11}$$

$$\begin{bmatrix} C_7 \\ C_8 \end{bmatrix}_{p+1} = \begin{bmatrix} 0 & 1 \\ 1 & 0 \end{bmatrix} \begin{bmatrix} C_7 \\ C_8 \end{bmatrix}_p \quad . \tag{A-12}$$

Now since

$$\hat{M} = \hat{O}_1 - \hat{O}_3 + \hat{O}_7 \quad , \tag{A-13}$$

the system is solved subject to the initial condition

$$C_1(1) = C_7(1) = 1 \quad , \quad C_3(1) = -1 \quad , \quad \text{all other } C_k(1) = 0 \; . \tag{A-14}$$

The simplest way to solve the 6-variable system is to expand the initial condition in terms of the eigenspectrum of the matrix transformation.

One finds the eigenvalues $\lambda = -1,\ +1,\ -2$ and $-\frac{1}{2}$ with -1 triply degenerate. Then applying the transformation $(p - 1)$ times to the initial condition easily gives the following solutions for the operator coefficents:

$$
\begin{aligned}
C_1(p) &= C_7(p) = \tfrac{1}{2}[1 - (-1)^p] \\
C_2(p) &= C_8(p) = \tfrac{1}{2}[1 + (-1)^p] \\
C_3(p) &= \tfrac{1}{3}[(-2)^p - 1] \\
C_4(p) &= -C_6(p) = -\tfrac{1}{6} + \tfrac{1}{2}(-1)^p - \tfrac{1}{3}(-2)^p \\
C_5(p) &= -\tfrac{1}{6} - \tfrac{1}{2}(-1)^p + \tfrac{1}{6}(-2)^p \quad .
\end{aligned}
\tag{A-15}
$$

Multiplying these by $K^p/p!$ and summing on p, the following operator result is found for $\hat{M} = \exp \hat{KM}$:

$$
\begin{aligned}
\hat{} &= 1 + \sinh K\,(\hat{O}_1 + \hat{O}_7) + (\cosh K - 1)(\hat{O}_2 + \hat{O}_8) \\
&\quad - \tfrac{1}{3}(e^{K} - e^{-2K})\hat{O}_3 + (\tfrac{1}{6}e^{K} - \tfrac{1}{2}e^{-K} + \tfrac{1}{3}e^{-2K})(\hat{O}_6 - \hat{O}_4) \\
&\quad + (\tfrac{1}{2} - \tfrac{1}{6}e^{K} - \tfrac{1}{2}e^{-K} + \tfrac{1}{6}e^{-2K})\hat{O}_5 \quad .
\end{aligned}
\tag{A-16}
$$

A calculation similar to the above gives the following expression for the other part of the Hamiltonian:

$$
\begin{aligned}
&\exp(-\beta\hat{V}_n/2m) = \exp(-\tfrac{1}{2}\alpha y_n^2 + \tfrac{1}{2}bz_n) \\
&= 1 + (e^{-\alpha/2} - 1)y_n^2 + b\gamma^{-1}e^{-\alpha/4} \sinh \gamma\, z_n \\
&\quad + [e^{-\alpha/4}(\cosh \gamma + \tfrac{1}{4}\alpha\gamma^{-1} \sinh \gamma) - 1](xyyx)_n \\
&\quad + [e^{-\alpha/4}(\cosh \gamma - \tfrac{1}{4}\alpha\gamma^{-1} \sinh \gamma) - e^{-\alpha/2}](yxxy)_n \quad , \\
&\gamma \equiv \tfrac{1}{2}(b^2 + \tfrac{1}{4}\alpha^2)^{1/2} \quad .
\end{aligned}
\tag{A-17}
$$

The nonzero matrix elements of $\hat{M}$, the isotropic exchange operator, are given here, where the notation is

$$\langle S_n^z S_{n+1}^z | \hat{M} | S_n^{z'} S_{n+1}^{z'} \rangle$$

$$\langle 00|M|00\rangle = \frac{1}{3}(2e^{K} + e^{-2K})$$

$$\langle 11|M|11\rangle = \langle -1-1|M|-1-1\rangle = e^{K}$$

$$\langle 01|M|01\rangle = \langle 10|M|10\rangle = \langle 0-1|M|0-1\rangle = \langle -10|M|-10\rangle = \cosh K$$

$$\langle 01|M|10\rangle = \langle 10|M|01\rangle = \langle 0-1|M|-10\rangle = \langle -10|M|0-1\rangle = \sinh K$$

$$\langle 00|M|1-1\rangle = \langle 1-1|M|00\rangle = \langle 00|M|-11\rangle = \langle -11|M|00\rangle = \frac{1}{3}(e^{K} - e^{-2K})$$

$$\langle 1-1|M|1-1\rangle = \langle -11|M|-11\rangle = \frac{1}{6}e^{K} + \frac{1}{2}e^{-K} + \frac{1}{3}e^{-2K}$$

$$\langle 1-1|M|-11\rangle = \langle -11|M|1-1\rangle = \frac{1}{6}e^{K} - \frac{1}{2}e^{-K} + \frac{1}{3}e^{-2K} \quad .$$

There are a total of 19 different nonzero vertex weights; all others are zero. When this interaction is combined with that due to the $\hat{V}_{n,n+1}$ term (symmetrized as in (12)), one finds that 41 of the posible 81 vertices are allowed. These allowed vertices are the only ones with an even number of 0's.

We also note that for arbitrary S, the isotropic exchange Hamiltonian will relate to a N_v-vertex model, where

$$N_v = 2(1 + 2^2 + 3^2 + \cdots + (2S)^2 + (2S + 1)^2 \quad ,$$

obtained by counting those vertices which conserve total magnetization between states. For example, S = 3/2 would be described by a 44-vertex model in the isotropic limit.

References

* Present Address: Department of Physics, The University of Florida, 215 Williamson Hall, Gainesville, FL 32611

1. H. J. Mikeska, J. Phys. C 11, L29 (1978); J. Appl. Phys. 52, 1950 (1981).
2. J. M. Loveluck, T. Schneider, E. Stoll and H. R. Jauslin, Phys. Rev. Lett. 45, 1505 (1980); J. Appl. Phys. 52, 1965 (1981); J. Phys. C 15, 1721 (1982).
3. O. G. Mouritsen, H. Jensen and H. C. Fogedby, Phys. Rev. B 30, 498 (1984).
4. G. Reiter, J. Appl. Phys. 52, 1961 (1981).
5. T. Schneider and E. Stoll, J. Appl. Phys. 53, 8024 (1982); Phys. Rev. B 22, 5317 (1980).
6. M. G. Pini and A. Rettori, Phys. Rev. B 29, 5246 (1984).
7. J. K. Kjems and M. Steiner, Phys. Rev. Lett. 41, 1137 (1978).
8. M. Steiner, K. Kakurai and J. K. Kjems, Z. Phys. B 53, 117 (1983).
9. T. Goto and Y. Yamaguchi, J. Phys. Soc. Japan 50, 2133 (1981).
10. A. P. Ramirez and W. P. Wolf, Phys. Rev. Lett. 49, 227 (1982); A. P. Ramirez, Ph.D. Thesis, Yale University (1984).
11. K. Kopinga, A. M. C. Tinus and W. J. M. de Jonge, Phys. Rev. B 29, 2868 (1984).
12. K. Kopinga, A. M. C Tinus and W. J. M. de Jonge, Phys. Rev. B 25, 4685 (1982).
13. J. P. Boucher, L. P. Regnault, J. Rossat-Mignod, J. P. Renard, J. Bouillot and W. G. Stirling, Solid State Comm. 33, 171 (1980); J. Appl. Phys. 52, 1956 (1981); L. P. Regnault, J. P. Boucher, J. Rossat-Mignod and J. P. Renard, J. Phys. C 15, 126 (1982).

14. J. F. Currie, J. A. Krumhansl, A. R. Bishop and S. E. Trullinger, Phys. Rev. B 22, 477 (1980).

15. P. Kumar, Phys. Rev. B 25, 483 (1982); Physica 5D, 359 (1982); E. Magyari and H. Thomas, Phys. Rev. B 25, 531 (1982); J. Phys. C 16, L535 (1983).

16. H. J. Mikeska and K. Osano, Z. Phys. B 52, 111 (1983).

17. G. Wysin,. A. R. Bishop and P. Kumar, J. Phys. C 15, L337 (1982); J. Phys. C 17, 5975 (1984).

18. R. Liebmann, M. Schöbinger and D. Hackenbracht, J. Phys. C 16, L633 (1983).

19. F. Borsa, M. G. Pini, A. Rettori and V. Tognetti, J. Magn. Magn. Mat. 31-34, 1287 (1983).

20. A. M. C. Tinus, W. J. M. de Jonge and K. Kopinga, preprint (1985).

21. K. Maki and H. Takayama, Phys. Rev. B 20, 3223 (1979); K. Maki, Phys. Rev. B 24, 3991 (1981); H. J. Mikeska, Phys. Rev. B 26, 5213 (1982).

22. Michael Durnan Johnson and Nancy Faye Wright, Phys. Rev. B 32, 5798 (1985).

23. M. Fowler and X. Zotos, Phys. Rev. B 24, 2634 (1981); 25, 2805 (1982).

24. K. Sasaki and T. Tsuzuki, J. Magn. Magn. Mat. 31-34, 1283 (1983).

25. P. Kumar and V. K. Samalam, Phys. Rev. Lett. 49, 1278 (1982).

26. M. Suzuki, Prog. Th. Phys. 56, 1454 (1976); M. Barma and B. S. Shastry, Phys. Rev. B 18, 3351 (1978).

27. M. Suzuki, S. Miyashita and A. Kuroda, Prog. Th. Phys. 58, 1377 (1977); J. J. Cullen and D. P. Landau, Phys. Rev. B 27, 297 (1983).

28. G. M. Wysin, Ph.D. Thesis, Cornell University (1985).

29. H. Betsuyaku, Prog. Th. Phys. 73, 319 (1985); Phys. Rev. Lett. 53, 629 (1984).

30. I. Satija, G. Wysin and A. R. Bishop, Phys. Rev. B 31, 3205 (1985).

31. H. F. Trotter, Proc. Am. Math. Soc. 10, 545 (1959).

32. H. DeRaedt, A. Lagendijk and J. Fivez, Z. Phys. B 46, 261 (1982).

33. N. Metropolis, A. W. Rosenbluth, M. N. Rosenbluth, A. H. Teller, and E. Teller, J. Chem. Phys. 21, 1087 (1953).

34. I. Morgenstern and K. Binder, Phys. Rev. B 22, 288 (1980).

35. J. C. Bonner and M. E. Fisher, Phys. Rev. 135, A640 (1964).

36. M. Suzuki, Phys. Rev. B 31, 2957 (1985).

37. T. Tsuzuki, Prog. Th. Phys. 73, 1352 (1985).

Figure Captions

Fig. 1 Representative spin-1 QMC data for $CsNiF_3$ parameters, using 16 spins and $m \simeq 60K/T$. The drawn curves are least square polynomial fits to the QMC averages, for in-plane fields 0 kG (0, solid), 5 kG (Δ, dashed) and 10 kG (+, dotted). All quantities are per spin.

Fig. 2 The differences $\Delta U = U(B) - U(0)$ and $\Delta C = C(B) - C(0)$ verses temperature, derived from Fig. 1a and Fig. 1b, for fields 5 kG (Δ, dashed) and 10 kG (+, dotted). The drawn curves are the differences of the least square polynomial fits in Fig. 1, while the data points are obtained by direct subtraction of the Fig. 1 data points.

Fig. 3 The differences $\Delta C = C(B) - C(0)$ verses B, as obtained from the spin-1 QMC calculation for $CsNiF_3$ parameters (see text). The data points correspond to temperatures 5K (◇), 6K (x), 7K (+), 8K (Δ) and 9K (0). There are only vague peaks in each set of data at fixed temperature, although these represent averages over $5 \times 192{,}000$ states.

Fig. 4 Field B_{peaks}, at which ΔC vs. B is maximum, verses T^2, from experimental and model calculations. The dashed line is a linear fit to the Ramirez and Wolf[10] experimental data for $CsNiF_3$. The data points are rough estimates from the QMC calculation, and the solid line is a linear fit to those data. The dashed line is the prediction of classical sG theory of Sasaki and Tsuzuki,[24] which includes effects of soliton-soliton interactions, as well as multiple spin wave and spin wave-soliton processes.

Fig. 5 An example of the extrapolation to $N \to \infty$, $m \to \infty$, for the specific heat per particle C/N, as used in the spin-1/2 QTM calculation. (Similar curves can be obtained for the internal energy, and in-plane magnetization and susceptibility.) CHAB parameters are used here; $J_x = J_z = 110$ K, $J_y = 104.5$ K. The in-plane field is $B_z = 5.5$ kG, and the temperature is $T \approx 7.20$ K. (a) Extrapolations to $N \to \infty$ at fixed values of $m = 3$ (□), $m = 5$ (0), $m = 7$ (Δ) and $m = 9$ (+). The straight lines are weighted least square fits. (b) Extrapolation to $m \to \infty$, using $3 \leq m \leq 9$. The data points are the values already extrapolated to $N \to \infty$, as found from the intercepts of curves as in (a). The straight line is a weighted least squares fit.

Fig. 6 Some typical results for ΔC vs. B as obtained with the spin-1/2 QTM calculation using CHAB parameters (5% anisotropy). The data correspond to temperatures T = 4.0 K (∇), 4.4 K ( ), 4.9 K (x), 5.5 K (+), 6.2 K (Δ) and 7.2 K (0), and have been extrapolated to $N \to \infty$, $m \to \infty$.

Fig. 7 Spin-1/2 QTM results for (a) B_{peak} and (b) ΔC_{max}, using model (2) with $J_x = J_z = 110$ K, for a series of values of anisotropy $J_y/J_x = 0.96$ (□), 0.95 (0), 0.94 (Δ), 0.92 (+) and 0.90 (x). These are all data from the extrapolation to $N \to \infty$, $m \to \infty$. The solid data points (•) are the experimental data on CHAB by Tinus et al.[20] The dashed lines are the classical sG theory of Sasaki and Tsuzuki.[24]

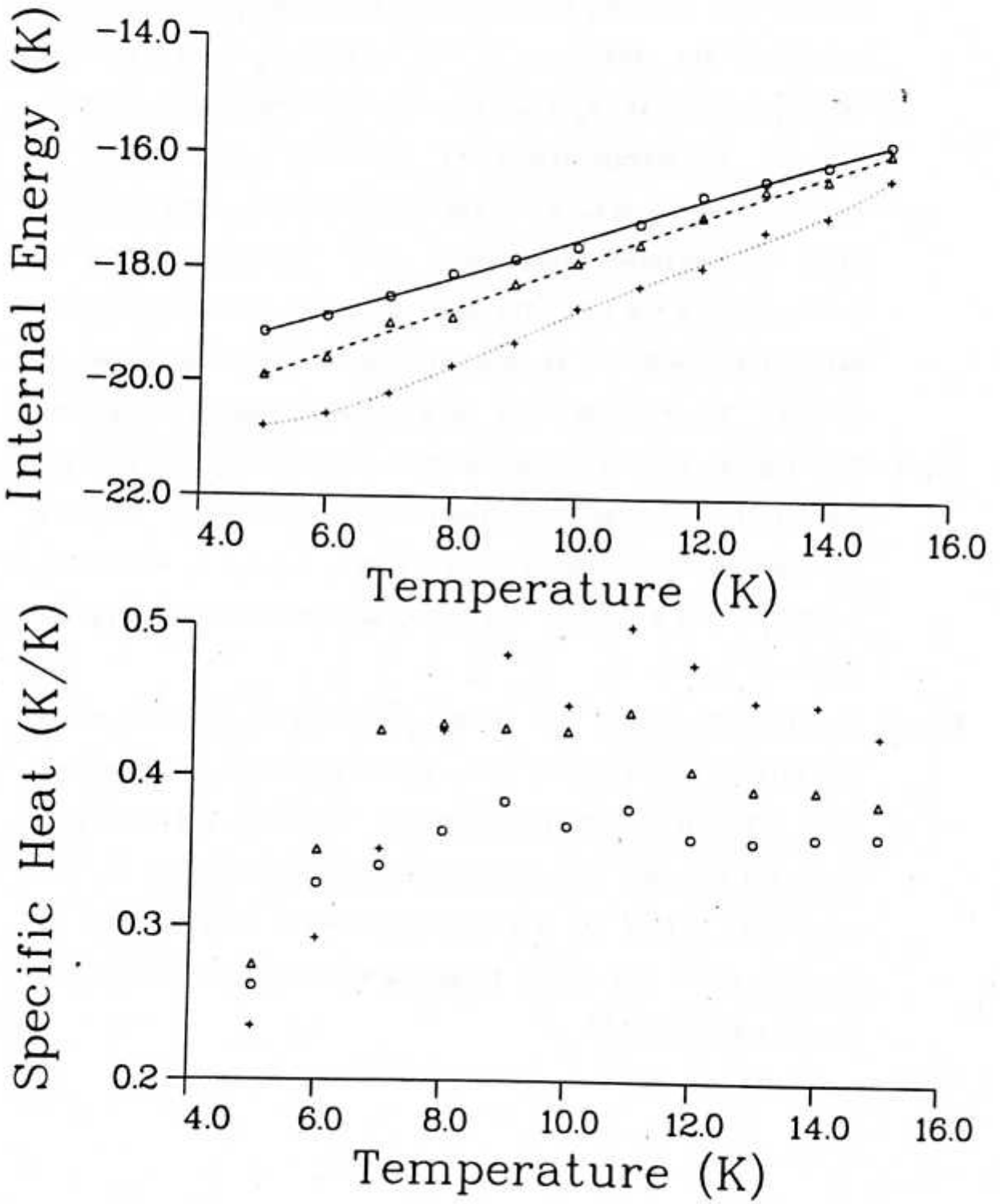
Internal Energy (K)
-14.0
-16.0
-18.0
-20.0
-22.0
4.0
6.0
8.0
10.0
12.0
14.0
16.0
Temperature (K)
Specific Heat (K/K)
0.5
0.4
0.3
0.2
4.0
6.0
8.0
10.0
12.0
14.0
16.0
Temperature (K)

Fig 1a.

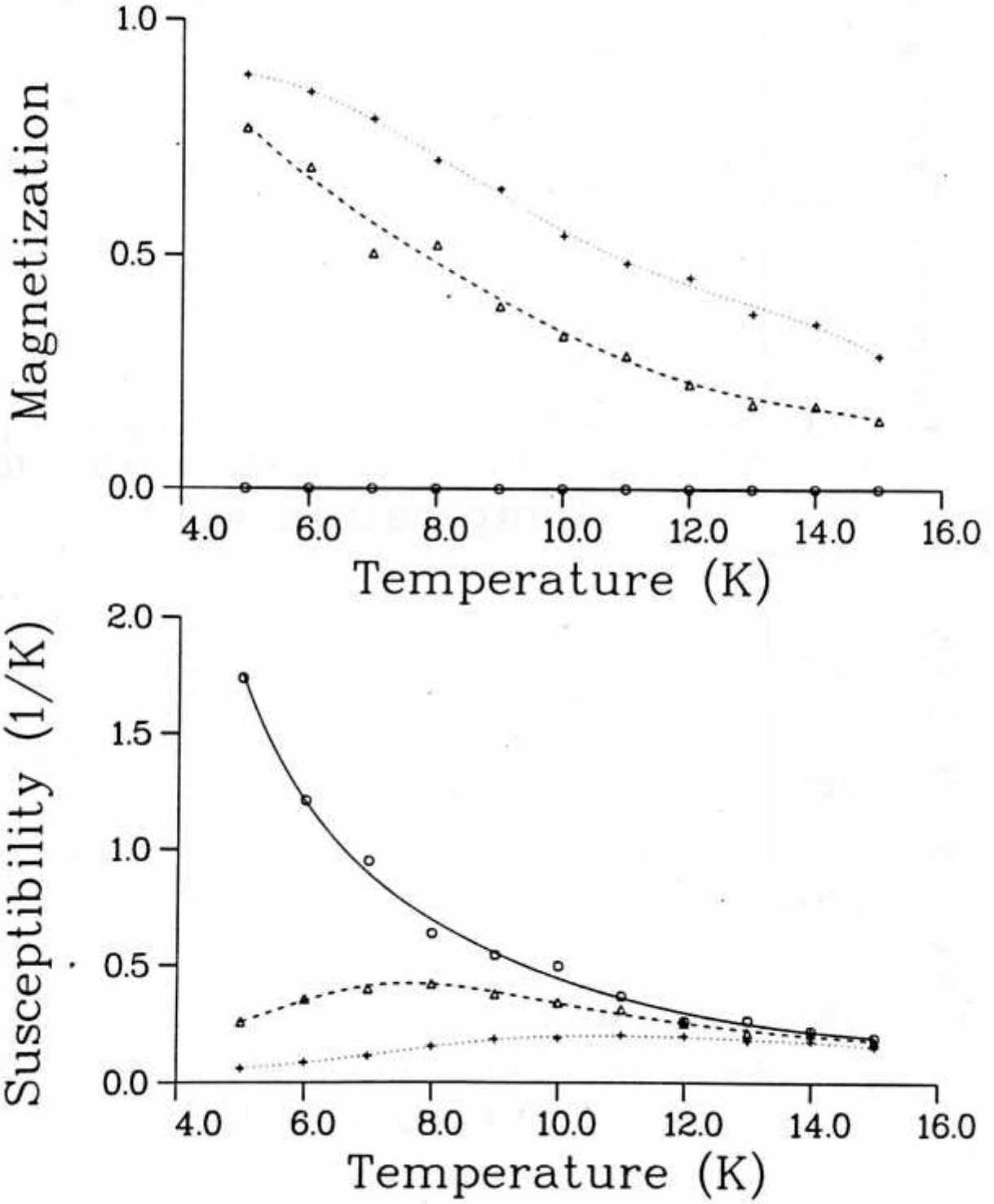
Magnetization
1.0
0.5
0.0
4.0
6.0
8.0
10.0
12.0
14.0
16.0
Temperature (K)
Susceptibility (1/K)
2.0
1.5
1.0
0.5
0.0
4.0
6.0
8.0
10.0
12.0
14.0
16.0
Temperature (K)

Fig 1b.

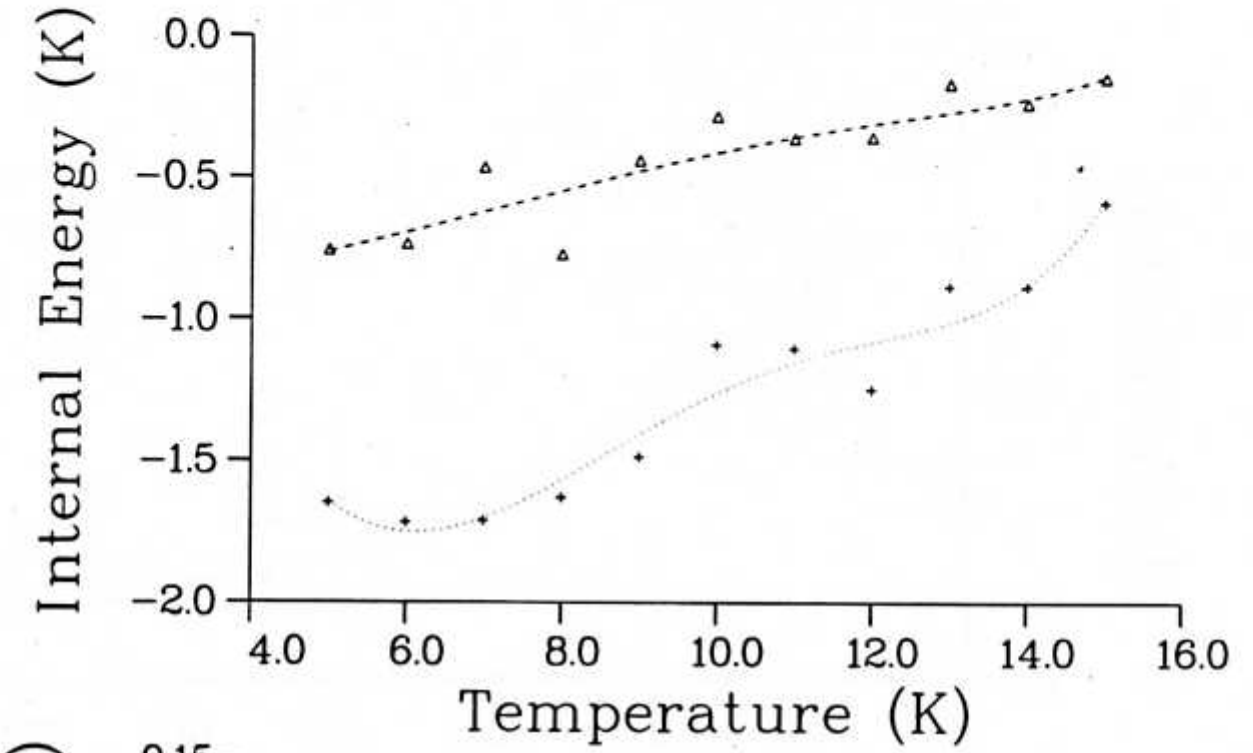
Internal Energy (K)
0.0
−0.5
−1.0
−1.5
−2.0
4.0
6.0
8.0
10.0
12.0
14.0
16.0
Temperature (K)

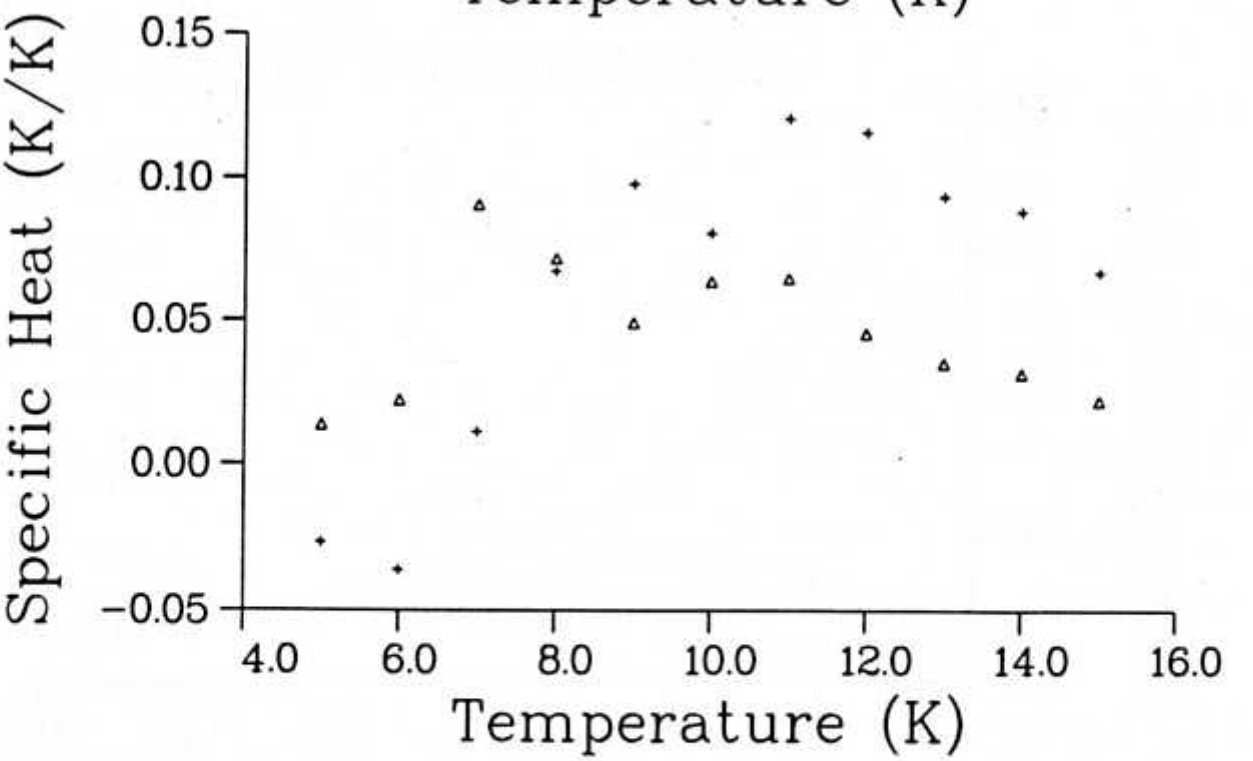
Specific Heat (K/K)
0.15
0.10
0.05
0.00
−0.05
4.0
6.0
8.0
10.0
12.0
14.0
16.0
Temperature (K)

Fig 2.

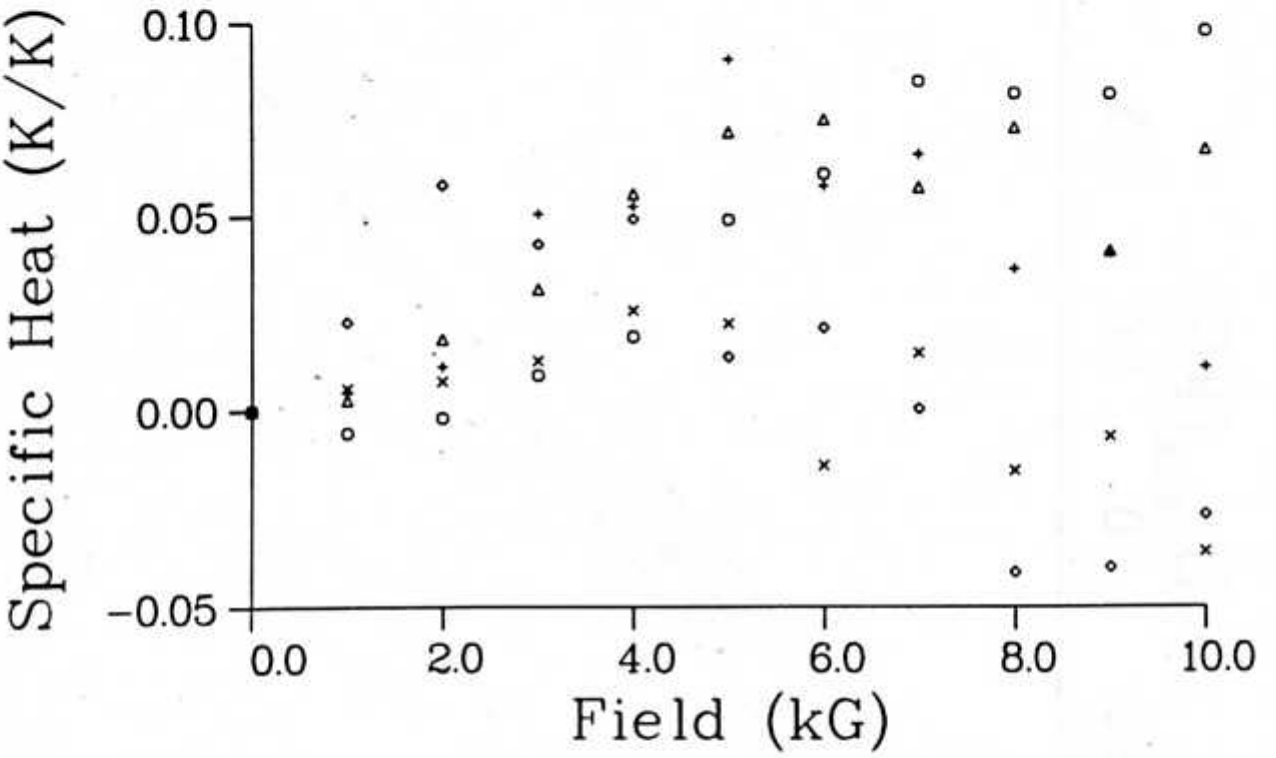

Fig 3.

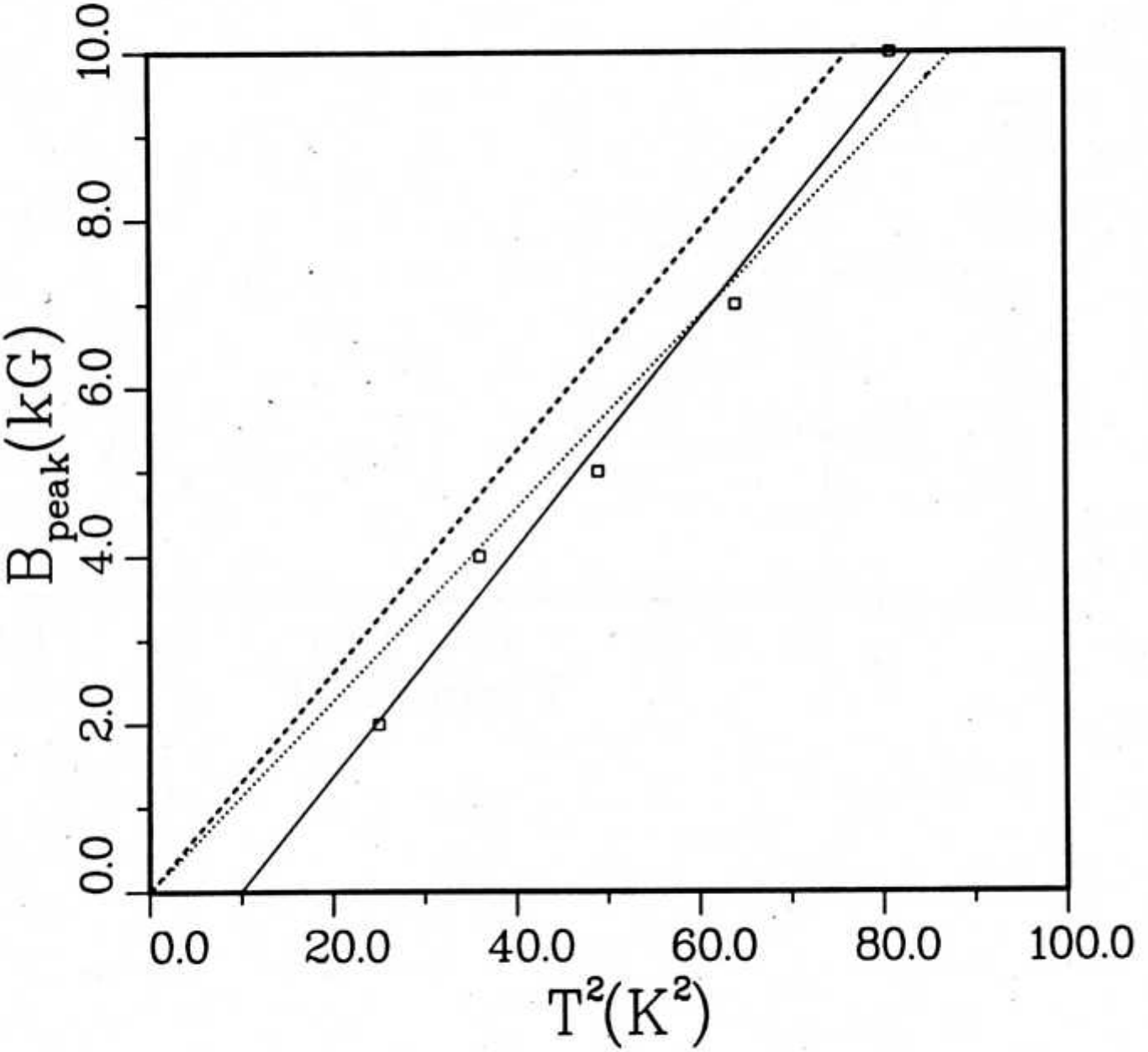

Fig 4.

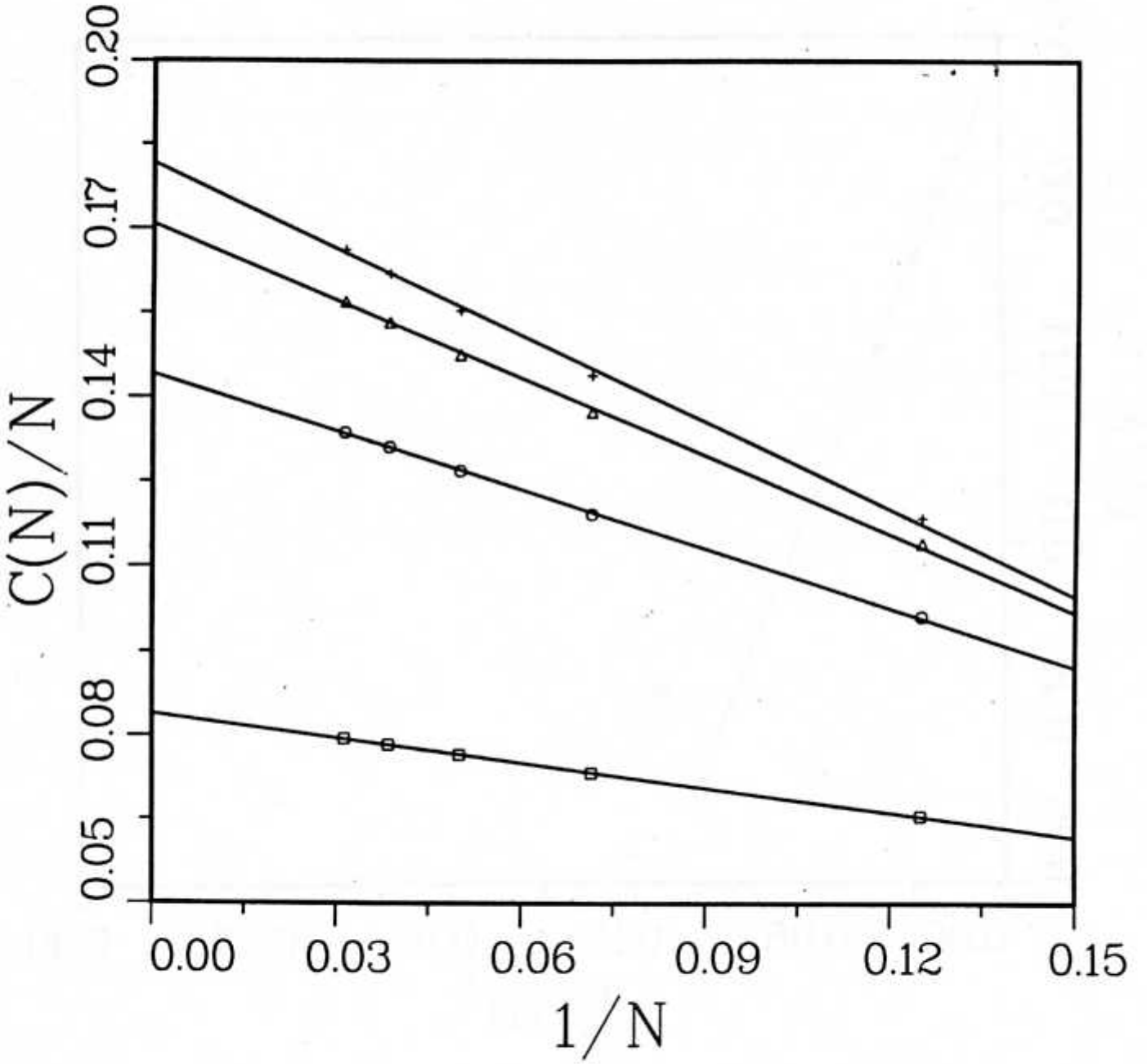

Fig 5a.

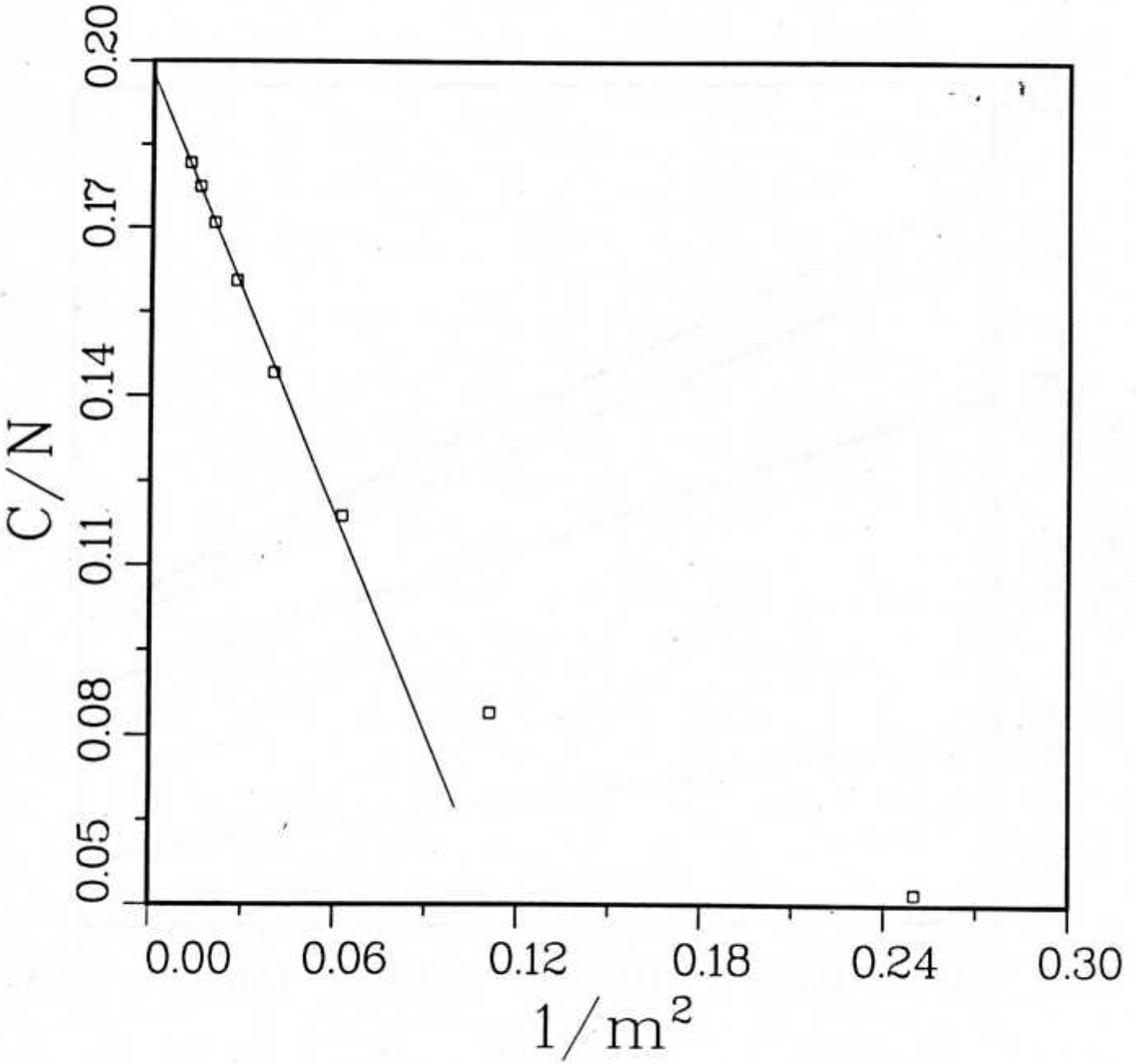

Fig 5b.

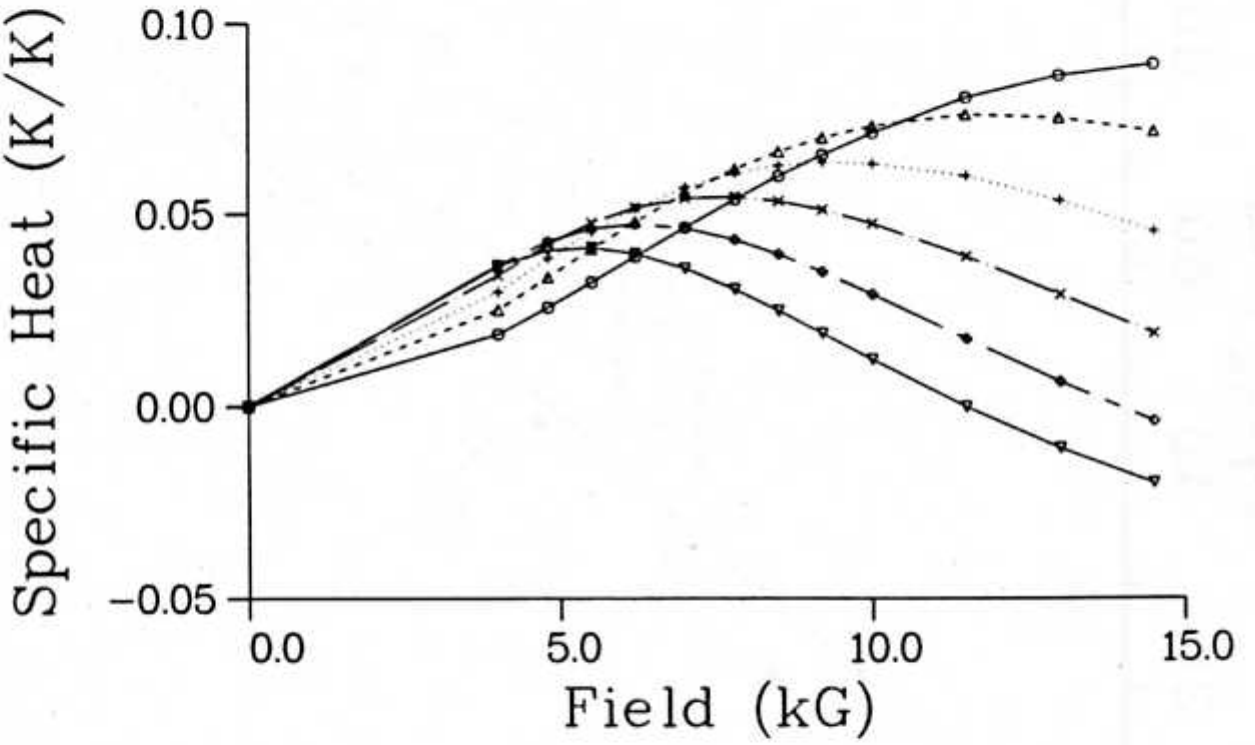

Fig 6.

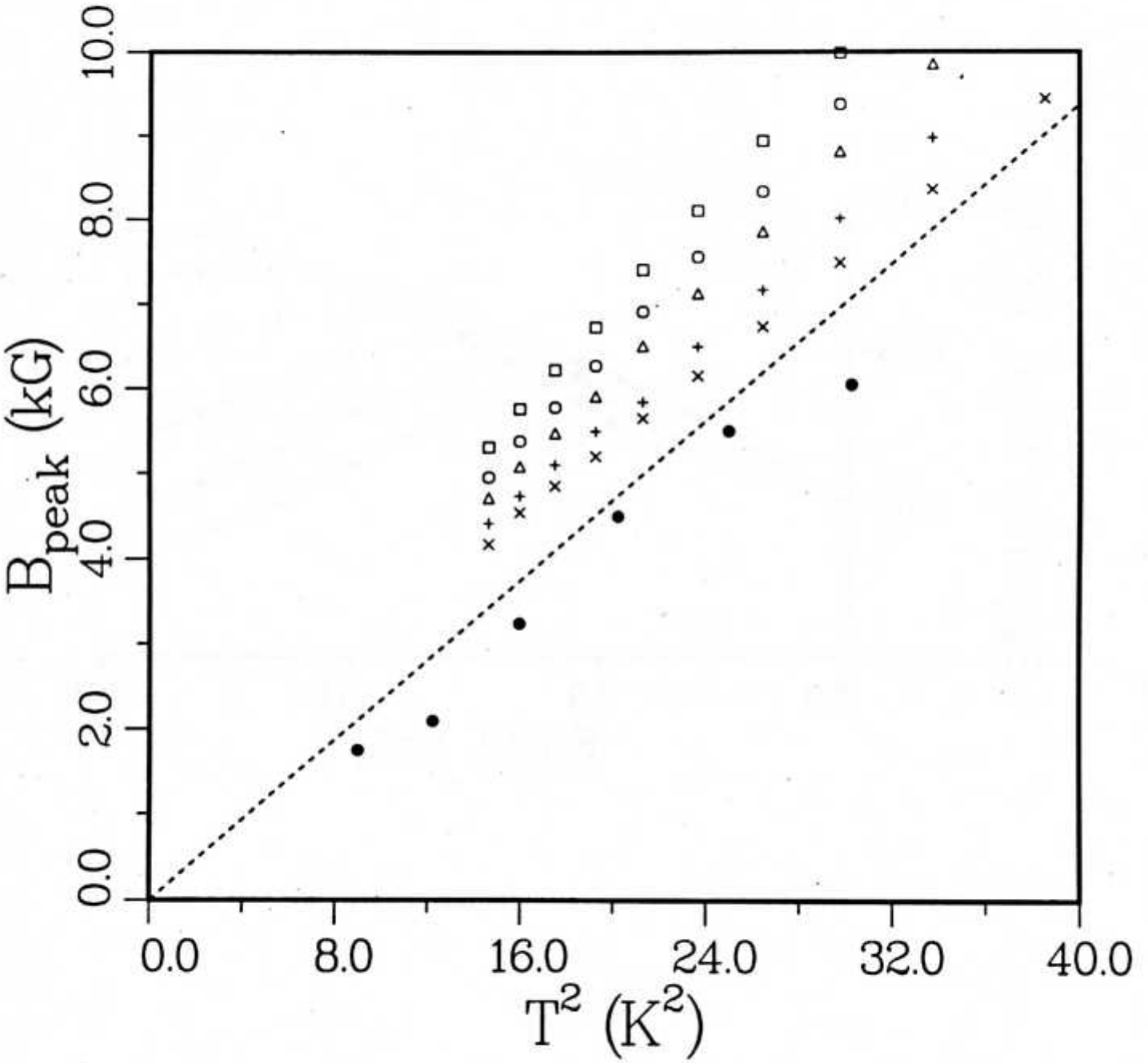

Fig 7a.

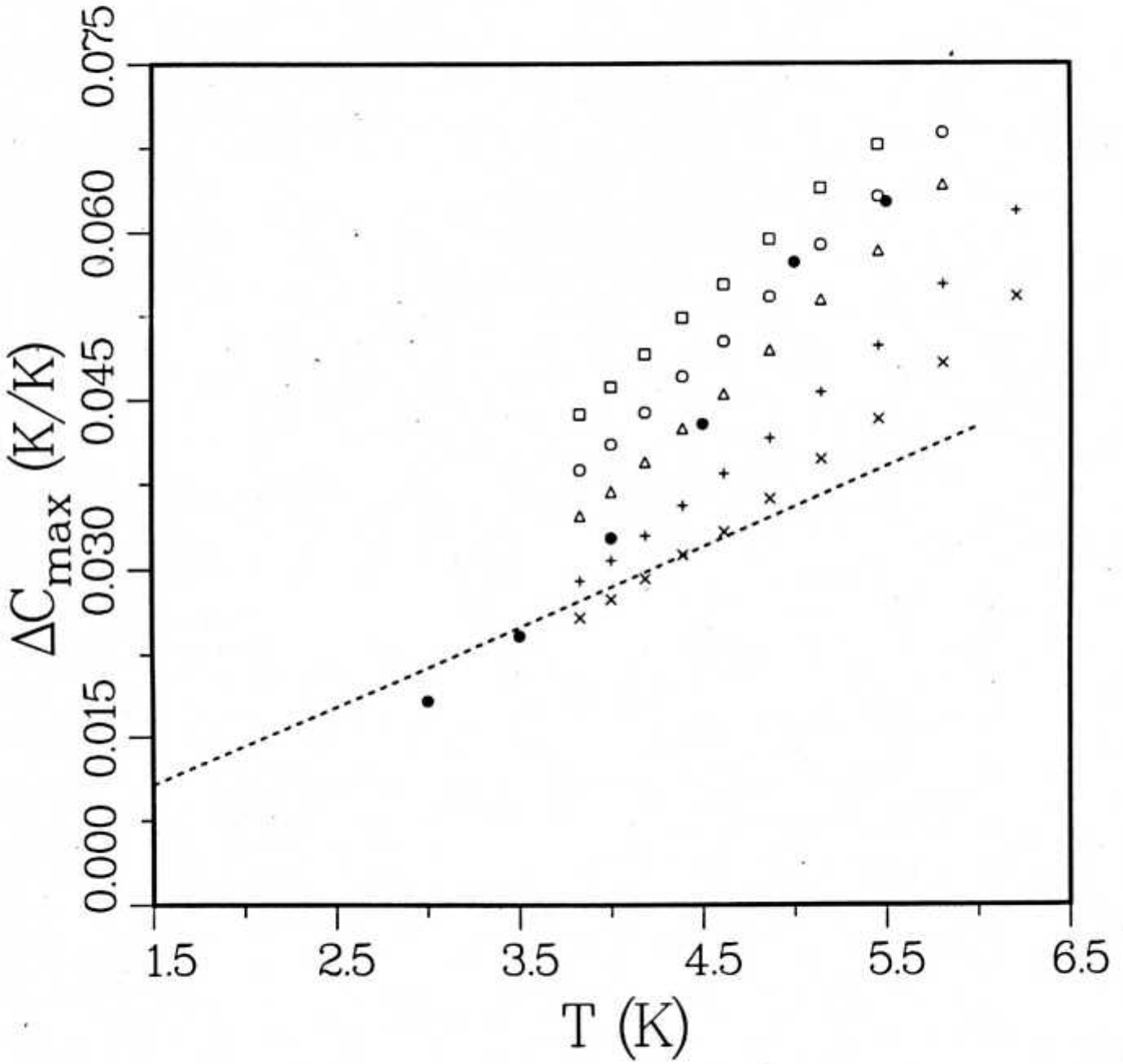

Fig 7b.